Optimization of 3-hole-assisted PMMA optical fiber with double cladding for UV-induced FBG fabrication

Kei-Chun Davis Cheng,[1,*] Ming-Leung Vincent Tse,[1] Guiyao Zhou,[1,2] Chi-Fung Jeff Pun,[1] Wing-Kin Edward Chan,[1] C. Lu[3], P. K. A. Wai,[3] and Hwa-yaw Tam[1]

[1]Photonics Research Centre, Department of Electrical Engineering, The Hong Kong Polytechnic University, Hung Hom, Kowloon, Hong Kong SAR, China
[2]Key Laboratory of Metastable Materials Science & Technology, Yanshan University, Hebei Province, China
[3]Photonics Research Centre, Department of Electronics and Information Engineering, The Hong Kong Polytechnic University, Hung Hom, Kowloon, Hong Kong SAR, China
[*]Corresponding author: eedavis@polyu.edu.hk

Abstract: We propose a new hole-assisted polymer optical fiber design to eliminate the influence of dopant diffusion and to increase the UV writing efficiency in fiber Bragg grating inscription. The optical waveguide is formed inside a solid core surrounded by a ring of 3 large air holes in enhanced UV photosensitive PMMA with double-cladding. We determined a map of the single-mode and multi-mode phase transitions using a finite-element–based vectorial optical mode solver. We obtained a wide range of geometrical configuration for the single-transverse-mode (HE11) propagation in the visible. The design is optimized to operate at the minimum optical loss wavelengths of 580 nm and 770 nm.

©2009 Optical Society of America

OCIS codes: (060.2280) Fiber design and fabrication; (060.4005) Microstructured fibers; (060.3738) Fiber Bragg gratings, photosensitivity

References and links

1. H. Dobb, D. J. Webb, K. Kalli, A. Argyros, M. C. J. Large, and M. A. van Eijkelenborg, "Continuous wave ultraviolet light-induced fiber bragg gratings in few- and single-moded microstructured polymer optical fibers," Opt. Lett. **30**, 3296-3298 (2005).
2. H. Y. Liu, H. B. Liu, G. D. Peng, and P. L. Chu, "Observation of Type I and Type II gratings behaviour in polymer optical fiber," Opt. Commun. **220**, 337-343 (2003).
3. J. M. Yu, X. M. Tao, and H. Y. Tam, "Trans-4-stilbenemethanol-doped photosensitive polymer fibers and gratings," Opt. Lett. **29**, 156-158 (2004).
4. J. M. Yu, X. M. Tao, and H. Y. Tam, "Fabrication of UV sensitive single-mode polymeric optical fiber," Opt. Mater. **28**, 181-188 (2006).
5. X. M. Tao, J. M. Yu, and H. Y. Tam, "Photosensitive polymer optical fibers and gratings," Trans. of the Institute of Meas. and Cont, **29**, 255-270 (2007).
6. H. Y. Tam, G. Y. Zhou, and C. F. Pun, "Method of fabricating polymer optical fiber preform for polymer optical fibers," *US patent* Application No. 12/329, 545.
7. H. Rogier, "Berenger and leaky mode in optical fibers terminated with a perfectly matched layer," J. Lightwave Technol. **20**, 1141-1148 (2002).
8. G. B. Ren, Z. Wang, S. Q. Lou, and S. S. Jian, "Mode classification and degeneracy in photonic crystal fibers," Opt. Express. **11**, 1310-1321 (2003).
9. H. P. Uranus, H. J. W. M. Hoekstra, and E. Groesen, "Mode of an endlessly single-mode photonic crystal fiber: a finite element investigation," *Proc. Symp. IEEE/LEOS Benelux Chapter* 311-314 (2004).
10. K. Iiyama, Z. Yamashita, and S. Takamiya, "Design of dispersion flattened photonic crystal fiber with a large core and a concentric missing ring," *Proc. of WFOPC2005 - 4th IEEE/LEOS Workshop on Fibers and Optical Passive Components* 10-13 (2005).
11. R. E. Wagner and W. J. Tomlinson, "Coupling efficiency of optics in single-mode fiber components," Appl. Opt. **21**, 2671-2688 (1982).

#105414 - $15.00 USD Received 16 Dec 2008; revised 22 Jan 2009; accepted 23 Jan 2009; published 2 Feb 2009
(C) 2009 OSA

1. Introduction

Polymethyl methacrylate (PMMA) is the most commonly used material for microstructured polymer optical fibers (mPOFs), especially in fiber sensing applications because of its much lower cost and larger strain extendibility over silica. Fiber Bragg Grating (FBG) written in the PMMA mPOF was initially reported in 2005 [1]. However, it was reported that the presence of several rings of air holes in the mPOF cladding caused obvious scattering, resulting in significant reduction in the optical intensity of the UV writing beam. A long exposure of higher UV intensity laser source can be used to compensate for the loss of intensity due to the scattering but it is adversely susceptible to physical damage within the fiber core [2]. Moreover, dopant diffusion especially in polymer optical fibers raises a concern which affects the transmission properties inside the core. In view of these problems, we have carried out several research studies on the development of enhanced UV photosensitive polymers to improve the writing efficiency of FBGs in single-mode POFs in the past [3-6].

In this paper, we propose a new fiber design using enhanced UV photosensitive PMMA polymer for efficient FBG writing. The design having 3 air holes and double cladding features single mode propagation with low confinement loss as well as minimize scattering of UV writing-beam. It can also reduce influence of dopant diffusion at the core region. Furthermore, it possesses single mode guidance at visible wavelengths where low attenuation loss window of PMMA occurs.

In our work, a finite-element–method (FEM) based vectorial optical mode solver (Mode Solutions^{TM} by Lumerical) was used to study the fiber design. We investigated the modal behavior by tailoring the dimensions of the structure, such that the single mode propagation was found for maximum effective core size and bridge. Two operating wavelengths, 580 nm and 770 nm, were used in the simulation.

2. Design of a 3-hole-assisted PMMA optical fiber with double cladding

As illustrated in Fig. 1, the proposed design comprises of double-clad layers in which the inner cladding region is made of trans-4-stilbenemethanol (TS)-doped PMMA and the outer cladding is made of undoped PMMA. Inside the TS-doped region, the fiber core for the single mode propagation is formed by the 3 large surrounding air holes. The effective core is located far away from the proximity of the inner/outer cladding region, thus the influence of dopant diffusion (shown in Fig. 2) can be minimized. Figure. 2 shows that in the generic PMMA POF preform with no air hole, a significant dopant diffusion effect takes place from the core to the cladding during the polymerization of the core material.

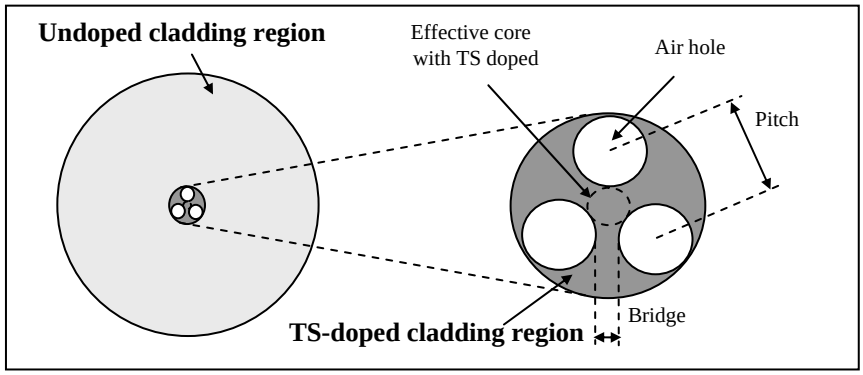

Fig. 1. Schematic Diagram of a PMMA hole-assisted fiber with a structure of 3-hole and double-clad.

#105414 - $15.00 USD Received 16 Dec 2008; revised 22 Jan 2009; accepted 23 Jan 2009; published 2 Feb 2009
(C) 2009 OSA

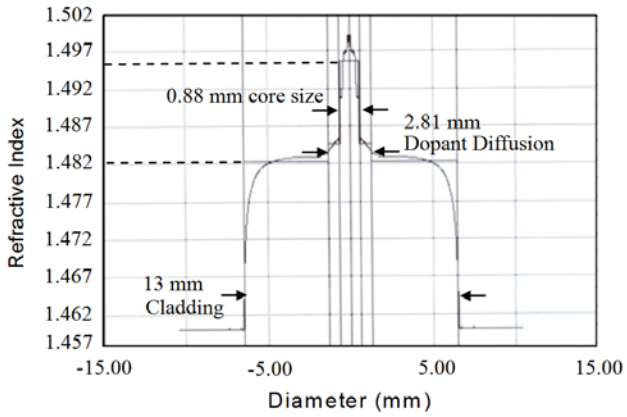

Fig. 2. Measured refractive index profile of a photosensitive POF preform determined by the 2600 Plastic Optical Fiber Preform Analyzer, Photon Kinetics, Inc.

3. Modal properties

The modal behaviour of the 3-hole-assisted PMMA optical fiber with double cladding were characterized by using the optical mode solver with circular perfectly-matched-layer (PML) boundary conditions [7]. The measured refractive index is depicted in Figure 3, and was used for the simulation. The index measurement was fitted with a single exponential-decay relation of the form:

$$n(\lambda) = A \cdot \exp(\frac{-\lambda}{t}) + B \tag{1}$$

Where n is the refractive index of PMMA, A is an initial value of refractive index, t is a decay constant, B is a minimum value of the refractive index and λ is the wavelength of light. A best fitting curve was obtained with the calculated parameters (A=1.670±0.153; B=1.493±0.001; t=90.476±2.869).

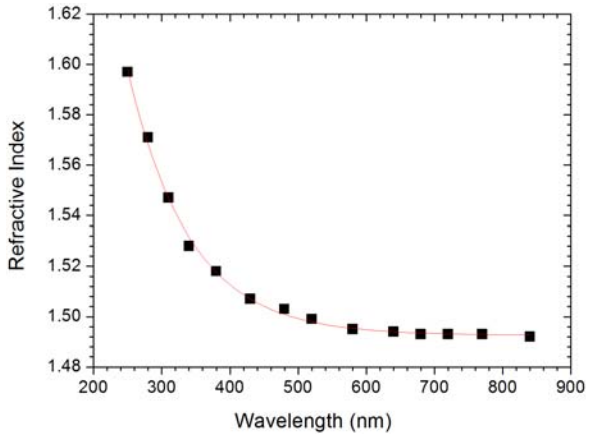

Fig. 3. Measured refractive index of the bulk TS-doped PMMA sample as a function of wavelength (250 – 850 nm) which is determined by the Spectroscopic Ellipsometer, Model GES-5E, SOPRA, Inc.

The vector plots of the transverse magnetic fields of each mode propagating in the structure (whose diameter of the effective core = 2.8 μm, bridge thickness = 1.35 μm, diameter of the air hole = 8 μm, diameter of TS-doped and undoped cladding regions = 19 μm

#105414 - $15.00 USD Received 16 Dec 2008; revised 22 Jan 2009; accepted 23 Jan 2009; published 2 Feb 2009
(C) 2009 OSA

and 40 μm, respectively) at the operating wavelength of 580 nm is depicted in Fig. 4. It is observed that multi-mode propagation with the first 5 modes (Fundamental mode: HE11a- and HE11b-like associated with next higher order modes: TE01-, TM01- and HE21-like) excite in the effective core. With group theoretical argument of n-fold rotation symmetry [8], HE11a- and HE11b-like modes are degenerate pairs with twofold polarization, shown in Figs. 4(a) and 4(b), whereas TE01- and TM01-like modes are non-degenerate pairs, shown in Figs. 4(c) and 4(d). HE21a- and HE21b-like modes are not readily distinguished in the structure and only one HE21 mode can be found, see Fig. 4(e).

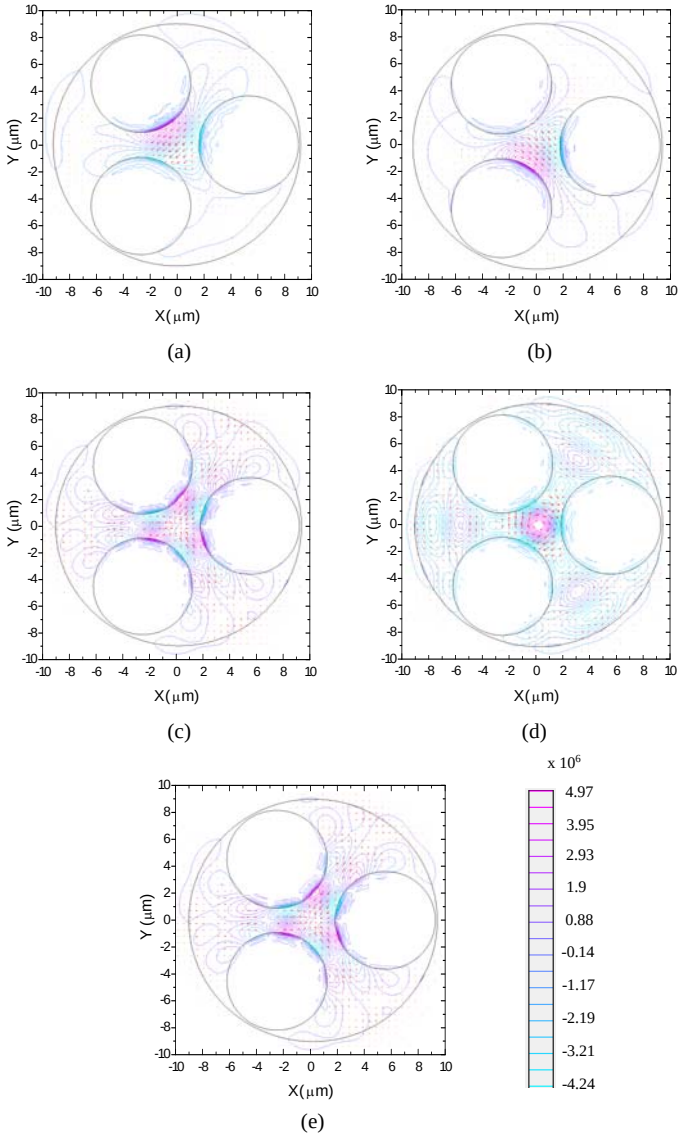

Fig. 4. The transverse magnetic fields of the first-five modes of the PMMA hole-assisted fiber with 3 holes. (a) HE11a-, (b) HE11b-, (c) TE01-, (d) TM01- and (e) HE21-like modes. (arrow denotes the field direction). The contour-line scale is in arbitrary unit.

The field distribution of the first 4 propagation mode groups is shown in Fig. 5. HE11-like mode in Fig. 5(a) that exhibits a Gaussian like field distribution with triangular shape inside the core is well confined in the core surrounded by the 3 air holes. This reveals that the

#105414 - $15.00 USD Received 16 Dec 2008; revised 22 Jan 2009; accepted 23 Jan 2009; published 2 Feb 2009
(C) 2009 OSA

confined mode excites far away from the inner/outer cladding boundary would not be affected by the persistent doping diffusion from TS-doped cladding region to the outer undoped region.

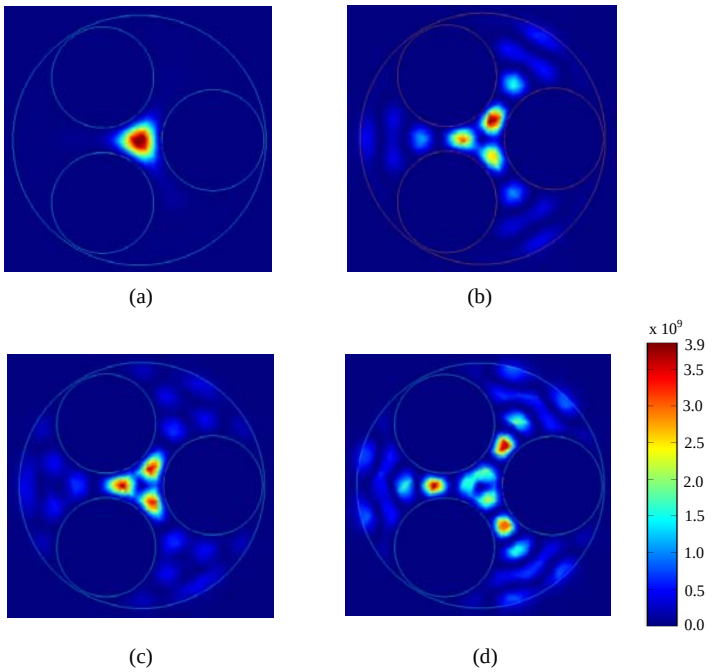

Fig. 5. The longitudinal component of the time averaged Poynting vector of (a) HE11-, (b) TE01-, (c) TM01-, (d) HE21 like modes of the 3-hole structure. The colour-coded scale is in arbitrary unit.

With known refractive indices of PMMA with TS-doped, their effective indices and confinement losses of the 5 propagation modes can be determined (shown in Table 1). The effective index of the HE11-like mode is well separated from the other modes and also the index of the bulk TS-doped PMMA. The associated confinement loss is at least 5 orders of magnitude (in dB scale) lower than that of the higher order modes. According to the multi-mode rejection ratio (MMRR) [9], this fiber geometry can be regarded as effectively single mode for long fiber-length application. The main application of the proposed fiber is in biomedical sensing where the fiber length is typically less than 10 meters. Thus the optimization of the design for strictly single mode operation is required.

Table 1. Effective refractive indices and confinement losses of first 5 propagation modes of the structure.

Mode	Effective Refractive Index	Confinement Loss (dB/m)
HE11a-like	1.48966	2.973e-10
HE11b-like	1.48965	1.479e-10
TE01-like	1.48456	2.925e-5
HE21-like	1.48433	3.352e-4
TM01-like	1.48398	1.132-5

4. Map of single mode phase transition

The study of cut-off wavelengths for the 3-hole-assisted PMMA optical fiber with different effective core diameters is investigated; the result is illustrated in Fig. 6(a). In this simulation, the air hole sizes vary, and the bridge thickness fixed at 1.1 μm. In Figs. 6(a) and 6(b), two

#105414 - $15.00 USD Received 16 Dec 2008; revised 22 Jan 2009; accepted 23 Jan 2009; published 2 Feb 2009
(C) 2009 OSA

curves of cut-off wavelengths represent the 2 phase transitions of the fundamental mode (HE11)- and the next higher order mode- cutoffs take place, creating a region of single mode propagation amid the two curves. For comparison, a generic PMMA POF with no holes is also shown. Fig. 6(b) shows that such fiber requires smaller core size to support single mode propagation at the same wavelength as that of the 3-hole-assisted fiber. Such small core fiber is difficult to be fabricated and it exacerbates the index variation due to the influence of doping diffusion at the doped/updoped boundary.

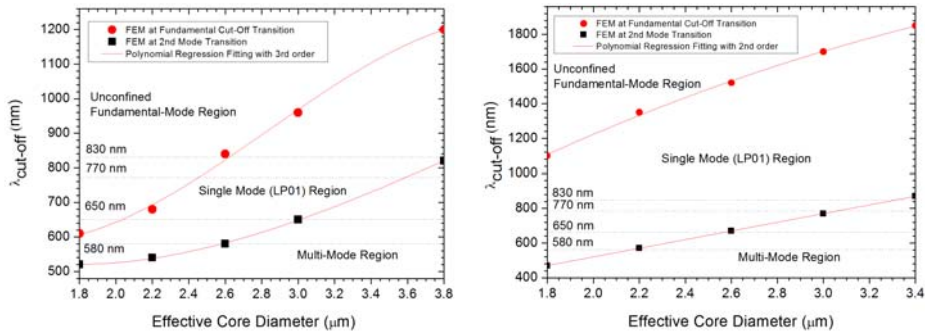

Fig. 6. Single mode phase transition as a function of an effective core diameter on (a) 3-hole-assisted PMMA optical fiber and (b) PMMA-based POF.

The effect of the bridge thickness on the cut-off wavelength is also investigated and the simulation results for the case of 2.6 μm and 3.4 μm effective core diameters are shown in Figs. 7(a) and 7(b), respectively. It is found that the bridge thickness whose the upper limit of two different core sizes are 1.46 μm and 1.83 μm, respectively. Beyond the limit, the bridge thickness is becoming so large that some unidentified spurious modes can quasi-confine inside the bridge, resulting in a deterioration of confinement loss scattering. The fundamental mode transition is less sensitive to the bridge thickness. Nevertheless, a wide region of single mode propagation is observed. These results along with that from Figs. 6(a) and 7(b) reveal that the tolerance of the core size and bridge thickness are sufficiently large (±16% and ±41%, respectively at a wavelength of 770 nm) for the single mode propagation. It alleviates the difficulty caused during the preform fabrication and fiber drawing process.

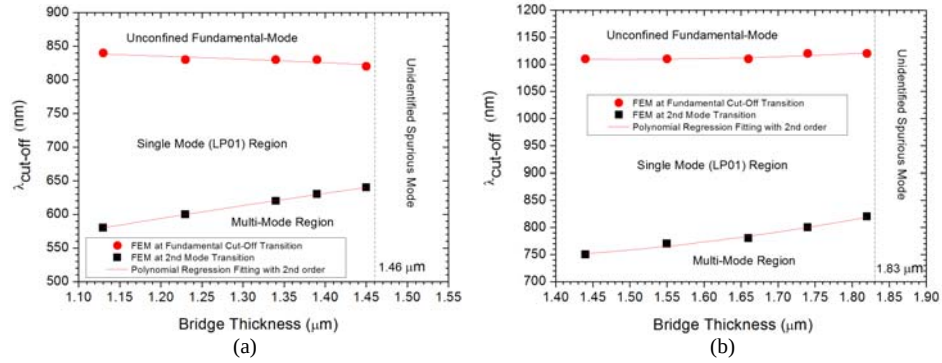

Fig. 7. Single mode phase transition as a function of bridge thickness on the 3-hole-assisted PMMA optical fiber with an effective core diameter of (a) 2.6μm and (b) 3.4μm, respectively.

5. Study of the effective mode area

Setting the bridge thickness to 1.1 μm, the effective mode area of the 3-hole-assisted PMMA optical fiber as a function of the effective core diameter within two phase transitions is investigated. The simulated effective mode area was calculated by [10]:

#105414 - $15.00 USD Received 16 Dec 2008; revised 22 Jan 2009; accepted 23 Jan 2009; published 2 Feb 2009
(C) 2009 OSA

$$A_{eff} = \frac{\left[\iint |E|^2 \, dxdy\right]^2}{\iint |E|^4 \, dxdy} \tag{2}$$

Where E is the amplitude of E-field intensity and can be determined by the Mode Solver.

The effective mode area moderately increases by broadening the bridge thickness to its upper limit as shown in Figs. 8(a) and 8(b).

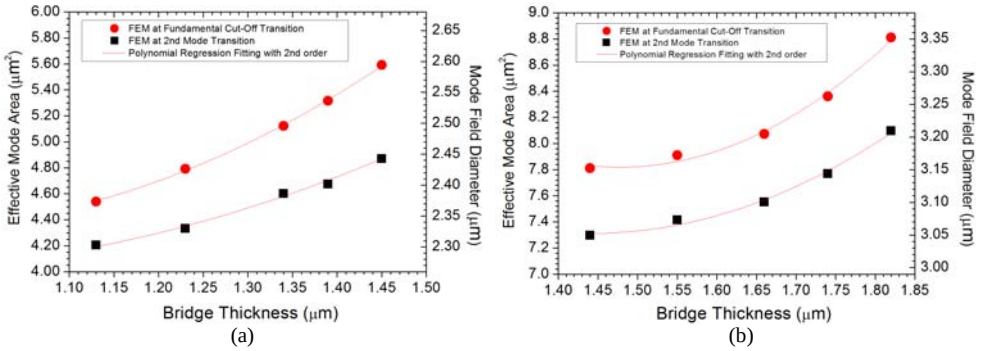

Fig. 8. Effective mode area and mode field diameter as a function of bridge thickness on the 3-hole-assisted PMMA optical fiber with an effective core diameter of (a) 2.6 μm and (b) 3.4 μm, respectively.

We calculated the power coupling efficiency between the 3-hole-assisted PMMA optical fiber, and a commercial single mode optical fiber (FiberCore SM600, with cut-off wavelength at 540 nm). The power coupling efficiency, T, was estimated by performing an overlap integral calculation using the formula [11]:

$$T = \sqrt{\frac{\left[\left|\int \vec{E}_{3-hole} \bullet \vec{E}_{SM\,600} dxdy\right|\right]^2}{\int \left|\vec{E}_{3-hole}\right|^2 dxdy \cdot \int \left|\vec{E}_{SM\,600}\right|^2 dxdy}} \tag{3}$$

where $E_{3\text{-}hole}$ and E_{SM600} are the electric field of the 3-hole-assisted PMMA optical fiber and SM-600, respectively. The E-field intensity can be determined by the Mode Solver.

As the effective core diameter of 3-hole-assisted PMMA optical fiber approaching to that of the SM600 (with effective mode area= 10.83 μm^2 and MFD= 3.7 μm), the coupling efficiency can be enhanced to 0.9, where the effective core diameter of the fiber is 3.4 μm.

6. Optimized parameter of the geometry

The effective core diameter and the bridge thickness for the 3-hole-assisted PMMA optical fiber operating at 580 nm and 770 nm were optimized according to the results discussed so far. The optimized fiber parameters are presented in Table 2. The optical properties are presented in Fig. 9 and Table 3. Figure 9(a) shows that the effective mode area of the fiber increases slightly with the TS-doped region diameter. This is because the effective mode area of the proposed fiber is strongly determined by the 3-hole configuration. In the simulation, the parameters of the 3 holes are kept constant. The confinement loss shown in Fig. 9(b) increases significantly with the inner cladding diameter, indicating that the confinement of the fundamental mode becomes weaken and thus introduces higher loss. Nevertheless, even if the cladding size is double from the optimized value, the confinement loss is still less than ~10^{-3} dB/m which can be negligible for most sensing applications.

#105414 - $15.00 USD Received 16 Dec 2008; revised 22 Jan 2009; accepted 23 Jan 2009; published 2 Feb 2009
(C) 2009 OSA

Table 2. Optimized dimensions of the 3-hole-assisted PMMA optical fiber at λ= 580 & 770 nm, respectively.

Optimized Dimensions	**Unit**	**580 nm**	**770 nm**
Outer Diameter of Undoped Cladding Region	μm	125.00	
Diameter of TS-Doped Cladding Region	μm	19.60	24.40
Diameter of Air Hole	μm	8.40	10.40
Pitch	μm	9.53	11.95
Bridge (max.)	μm	1.13	1.55
Air Filling Fraction	---	0.55	0.55
Effective Core Diameter (max.)	μm	2.60	3.40

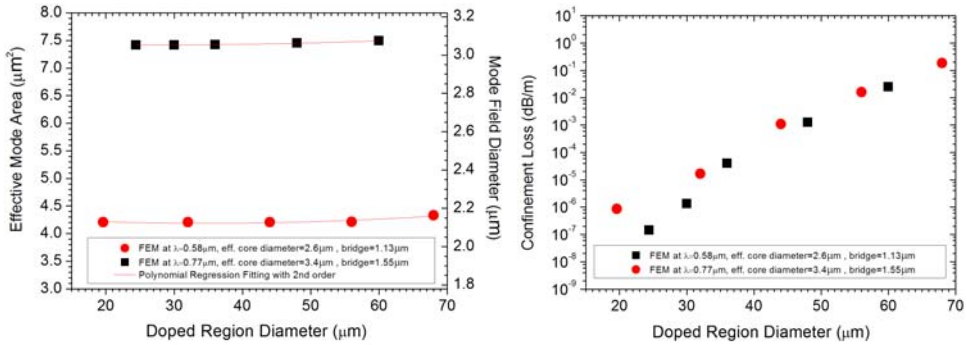

(a) (b)

Fig. 9. (a) Effective mode area and (b) confinement loss as a function of doped region diameter on the 3-hole-assisted PMMA optical fiber with an effective core diameter of 2.6 μm and 3.4 μm, respectively.

Table 3. Optical properties of the 3-hole-assisted PMMA optical fiber at λ= 580 & 770 nm, respectively.

Optical Properties	**Unit**	**580 nm**	**770 nm**
Operating Wavelength	μm	0.58	0.77
Refractive Index of PMMA (Doped)	---	1.495	1.493
Refractive Index of PMMA (Undoped)	---	1.483	1.482
Effective Refractive Index of LP01 mode	---	1.490	1.487
Confinement Loss	dB/m	6.351e-7	2.715e-7
Effective Mode Area of core (max.)	μm^2	4.206	7.415
Mode Field Diameter (MFD)	μm	2.314	3.073
Power Coupling to SM-600 standard fiber (Fiber core)	---	0.724	0.891
Insertion Loss	dB	1.403	0.501

7. Study of optical power field distribution

Optical power field distribution of the 3-hole-assisted PMMA optical fiber with optimized dimensions were characterized to investigate how an enhancement of the UV writing efficiency offered inside the effective core for FBG inscription. With a 2D simulation by Comsol FEMLAB, a plane wave of a wavelength of 325 nm (that is the UV writing wavelength) propagated transversally at normal incidence towards the microstructure inside the TS-doped cladding region. The field distribution in two different orientations of the microstructure is presented in Figs. 10(a) and 10(b). Figure 10(a) shows that the UV field lines can penetrate through the bridge and reach the effective core, resulting in a maximum optical power obtained. A uniform fringe pattern is observed inside the core region, led to an enhancement in UV writing efficiency. It can be speculated that only a few large air holes inside the photosensitive region would not introduce significant scattering. Figure 10(b) shows that when the plane wave normally propagated through a large air hole, optical power

#105414 - $15.00 USD Received 16 Dec 2008; revised 22 Jan 2009; accepted 23 Jan 2009; published 2 Feb 2009
(C) 2009 OSA

inside the effective core dropped significantly because of an existence of scattering and high contrast of refractive index between the solid core and air. Although the uniform fringe pattern can still be seen in the entire effective core, however, a reduction in optical power will reduce the efficiency of FBG inscription. More important, writing FBG through the holes require more UV energy leading to a larger increase in fiber's temperature during the grating fabrication process. This would have a degradation effect on the FBG thus fabricated.

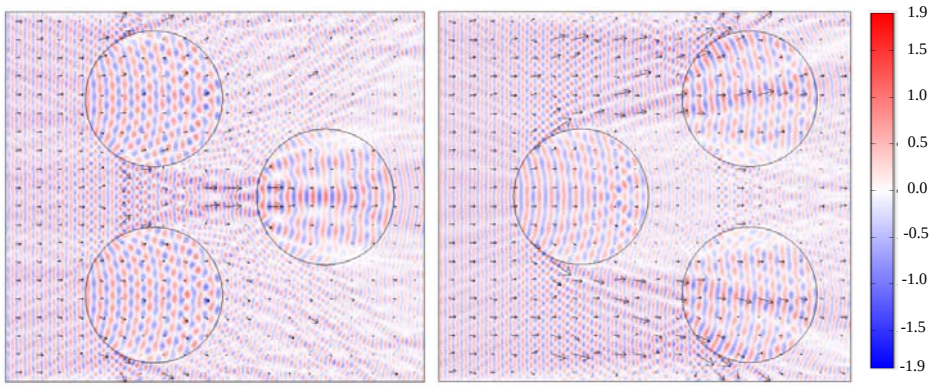

(a) (b)

Fig. 10. Optical power distribution across the 3-hole-assisted PMMA optical fiber after propagation of a plane wave at normal incidence transversally to the hole-assisted fiber. With a wavelength of 325 nm, the electric field propagated from left to right (arrow denotes the field direction). The colour-coded scale is in arbitrary unit.

8. Conclusions

We have proposed a new approach of optical fiber design in 3-hole-assisted PMMA optical fiber with double-cladding to eliminate the effect of dopant diffusion and to improve the UV writing efficiency. Its modal behavior excited inside the fiber was investigated so as to devise a relationship between the critical parameters such as cut-off wavelength, effective core diameter and bridge thickness. Effective mode area and power coupling were studied for the optimized design. The optimized parameters and the associated optical properties of the design operating at 580 nm and 770 nm were obtained, respectively. The fabrication of the fiber with the optimized geometry is carried out and further experimental work such as optical bending loss, UV FBG writing performance with uniformity of doping and sensitivity of temperature/strain with this fiber design will be reported afterwards.

Acknowledgments

The authors acknowledge the funding support from the University Grants Council's Matching Grant of the Hong Kong Special Administrative Region Government under the Niche Areas project J-BB9J and Central Research Grant of The Hong Kong Polytechnic University under Project G-U347.

#105414 - $15.00 USD Received 16 Dec 2008; revised 22 Jan 2009; accepted 23 Jan 2009; published 2 Feb 2009
(C) 2009 OSA